Published in final edited form as:
Nat Neurosci. 2013 November ; 16(11): 1662–1670. doi:10.1038/nn.3544.

A disinhibitory circuit mediates motor integration in the somatosensory cortex

Soohyun Lee[1], **Illya Kruglikov**[1], **Z Josh Huang**[2], **Gord Fishell**[1], and **Bernardo Rudy**[1]

[1]New York University Neuroscience Institute, Department of Neuroscience and Physiology, Smilow Research Center, New York University School of Medicine, New York, New York, USA

[2]Cold Spring Harbor Laboratory, Cold Spring Harbor, New York, USA

Abstract

The influence of motor activity on sensory processing is crucial for perception and motor execution. However, the underlying circuits are not known. To unravel the circuit by which activity in the primary vibrissal motor cortex (vM1) modulates sensory processing in the primary somatosensory barrel cortex (S1), we used optogenetics to examine the long-range inputs from vM1 to the various neuronal elements in S1. We found that S1-projecting vM1 pyramidal neurons strongly recruited vasointestinal peptide (VIP)-expressing GABAergic interneurons, a subset of serotonin receptor–expressing interneurons. These VIP interneurons preferentially inhibited somatostatin-expressing interneurons, neurons that target the distal dendrites of pyramidal cells. Consistent with this vM1-mediated disinhibitory circuit, the activity of VIP interneurons *in vivo* increased and that of somatostatin interneurons decreased during whisking. These changes in firing rates during whisking depended on vM1 activity. Our results suggest previously unknown circuitry by which inputs from motor cortex influence sensory processing in sensory cortex.

The exquisite ability of the neocortex to perform complex functions depends on dense interconnections between functionally related cortical areas. The superficial layers of cortex, often referred to as the associative layers, are a major target of these projections[1]. In the whisker-related somatosensorimotor system of rodents, the S1 and vM1 cortices are heavily interconnected[2–5]. These reciprocal connections between vM1 and S1 are thought to be important for sensorimotor integration and active sensing, contributing to the precise execution of motor tasks[6–8].

Correspondence should be addressed to B.R. (bernardo.rudy@nyumc.org) or S.L. (soohyun.lee@nyumc.org).

Note: Any Supplementary Information and Source Data files are available in the online version of the paper.

AUTHOR CONTRIBUTIONS

S.L., G.F. and B.R. conceived the study. S.L. conducted all of the ChR2 and NpHR experiments and analysis. I.K. conducted local input experiments and analysis, and set up two-photon targeted *in vivo* recordings. S.L. and I.K. performed *in vivo* experiments. Z.J.H. provided *Vip-cre* and *Sst-cre* mice. S.L., I.K., G.F. and B.R. wrote the paper.

COMPETING FINANCIAL INTERESTS

The authors declare no competing financial interests.

The axons of vM1 pyramidal neurons branch off in infragranular layers of S1, avoid the granular layer and extensively ramify in superficial layers[5]. These cortico-cortical interconnections in superficial layers are likely to be crucial for context-dependent sensory processing and sensorimotor integration[7,9,10].

However, an understanding of the circuit mechanisms by which motor activity in vM1 modulates sensory processing is currently lacking. In particular, the vM1 projections to GABAergic interneurons and the relative weight of these inputs as compared with those onto principal cells have not been reported[11,12]. Given the large diversity of interneurons and their role in the precise spatiotemporal control of excitatory outputs and cortical network dynamics, determining the afferent connectivity of vM1 onto S1 interneurons is critical for understanding how vM1 modulates S1 activity. Tantalizing support for this notion comes from studies demonstrating that the activity of distinct types of interneurons is differentially correlated with whisking behavior[13,14].

We previously found that interneurons expressing the ionotropic serotonin 5HT3a receptor (5HT3aR), together with parvalbumin (PV)-expressing and somatostatin (SST)-expressing neurons, can account for most, if not all, cortical GABAergic interneurons in S1. We also found that the 5HT3aR interneuron population is the largest group of GABAergic cells in the superficial layers of S1 (refs. 15,16). Although all 5HT3aR interneurons are uniformly modulated by serotonin and acetylcholine via ionotropic receptors and share the same developmental origin, the caudal ganglionic eminence, this population is heterogeneous. For example, it includes the neurogliaform interneurons[17–19] and the VIP-expressing interneurons[19,20]. The preponderance of 5HT3aR interneurons and the dense arborization of vM1 axons in S1 superficial layers suggest that 5HT3aR interneurons may be important for vM1 modulation of S1.

We examined the long-range inputs from vM1 to the various neuronal elements of S1 and found that S1-projecting vM1 pyramidal neurons strongly recruited VIP interneurons, one of the subtypes of 5HT3aR interneurons in S1 superficial layers, and, in turn, that VIP interneurons preferentially inhibited SST cells, GABAergic interneurons that target the distal dendrites of pyramidal cells. The existence of this circuit is supported by the observation that *in vivo* VIP interneurons were strongly and specifically activated during whisking, whereas SST interneuron activity was suppressed. Furthermore, inactivation of vM1 diminished these changes in VIP and SST interneuron activity during whisking, suggesting a causal link between vM1 activity and the effect of whisking on VIP and SST interneurons in S1 superficial layers. Taken together, our results describe previously unknown circuitry by which inputs from motor cortex influence activity in somatosensory cortex.

RESULTS

5HT3aR neurons in S1 receive strong excitatory input from vM1

To manipulate the activity of excitatory afferents from the vibrissal region of primary motor cortex (vM1), we expressed the light-sensitive cation channel channelrhodopsin 2 (ChR2) in vM1 of *Emx1-cre* mice using viral injection[21]. Emx1 is a pan-marker of pyramidal neurons

of the cerebral cortex and hippocampus[21]. Adeno-associated virus (AAV) directed the expression of ChR2 following Cre-mediated recombination[22]. ChR2 was specifically expressed in pyramidal neurons throughout the cortical layers of vM1 (Fig. 1). Photo-stimulation reliably elicited spikes from ChR2-expressing pyramidal neurons in vM1 with short latency (Supplementary Fig. 1). In S1, we observed ChR2-expressing vM1 axons in infragranular and supragranular layers and an especially dense arborization in layer 1 (Fig. 1a), consistent with previous studies[5]. However, axonal density and the anatomical superposition of axons and dendrites does not necessarily indicate the strength of synaptic connections[11,23].

To investigate the vM1 inputs onto the different cellular elements of S1 superficial layers, we used whole-cell recording to measure the postsynaptic responses evoked by photo-stimulation of ChR2-expressing vM1 axons. To target most interneuron subtypes, we used three lines of transgenic mice expressing GFP-labeled PV interneurons (B13), SST interneurons (GIN) and 5HT3aR interneurons (5HT3a^{eGFP})[15,24,25]. Together, 5HT3aR-, PV- and SST-expressing interneurons include close to 100% of supragranular interneurons[15,16]. Thus, recording synaptic weights of vM1 inputs to these three types of interneurons and to pyramidal cells allowed us to characterize the vM1 connections to all known cellular elements of the S1 superficial layers. We crossed these mouse lines with *Emx1-cre* mice to express ChR2 specifically in vM1 pyramidal neurons and simultaneously identify specific types of interneurons in S1. To control for the variability in the level of ChR2-expression in vM1 pyramidal neurons in different brain slices, we simultaneously recorded from an identified interneuron and a nearby pyramidal neuron (Fig. 1b). We normalized the photo-stimulation–evoked response in a given interneuron type to the response in the pyramidal neuron (Fig. 1b).

We found that vM1 axons provided similar excitatory inputs to fast-spiking interneurons and pyramidal neurons in S1. Photo-stimulation of vM1 axons evoked excitatory postsynaptic currents (EPSCs) of equivalent amplitudes in a representative fast-spiking interneuron and pyramidal neuron (fast spiking, −75.69 ± 3.03 pA; pyramidal, −81.07 ± 2.97 pA; $P = 0.1$, Mann-Whitney *U* test; Fig. 1c). Similarly, current-clamp recordings revealed that the excitatory postsynaptic potentials (EPSPs) evoked by photo-stimulation were of similar amplitude in these two types of neuron (fast spiking, 5.22 ± 0.51 mV; pyramidal, 6.01 ± 0.64 mV, $P = 0.18$, Mann-Whitney *U* test; Fig. 1c). Population data indicated that vM1 provided a similar degree of excitatory inputs onto fast-spiking and pyramidal neurons in S1 superficial layers (fast spiking to pyramidal ratio, mean = 0.97 ± 0.76, median = 0.38, $P = 0.08$, Wilcoxon signed-rank test; Fig. 1f,g). We also observed a similar degree of synaptic depression resulting from paired-pulse photo-stimulation (5 Hz) in both fast-spiking and pyramidal neurons (paired-pulse ratio: fast spiking, 0.90 ± 0.17; pyramidal, 0.95 ± 0.10).

We found that vM1 axons provided substantially stronger inputs to 5HT3aR interneurons. Photo-stimulation–evoked EPSCs were significantly larger in a 5HT3aR interneuron than in a pyramidal neuron (5HT3aR, −523.61 ± 7.01; pyramidal, −80.53 ± 12.42 pA; $P < 0.001$, Mann-Whitney *U* test; Fig. 1d). Under current-clamp mode, photo-stimulation reliably elicited spikes from the 5HT3aR interneuron, yet the same stimulation evoked only subthreshold depolarization in the nearby pyramidal neuron (5HT3aR, 21.67 ± 0.11 mV;

pyramidal, 5.52 ± 0.47 mV; $P < 0.001$, Mann-Whitney U test; Fig. 1d,f). Significantly larger excitatory inputs to 5HT3aR interneurons were consistently found across the population. On average, 5HT3aR interneurons received vM1 inputs that were more than twice as large as those received by pyramidal neurons (5HT3aR to pyramidal ratio, 2.33 ± 1.02, $P < 0.001$, Wilcoxon signed-rank test; Fig. 1f). The observed differences in the responses to vM1 inputs between 5HT3aR interneurons and other types of neurons were even greater when recorded under current clamp (Fig. 1g). Excitatory inputs from vM1 led to spiking activity in 30% of 5HT3aR interneurons (7 of 21 5HT3aR interneurons), yet we did not observe EPSP in other types of neurons reaching spike threshold in response to the same photo-stimulation. 5HT3aR interneurons had significantly higher resting membrane potentials and membrane input resistance (Supplementary Fig. 2). These factors, in addition to stronger vM1 inputs, are likely responsible for the larger membrane depolarization in 5HT3aR interneurons. Paired-pulse stimulation resulted in synaptic depression in the 5HT3aR interneurons (paired-pulse ratio, 0.90 ± 0.17), similar to that observed in fast-spiking interneurons and pyramidal cells.

We found that SST interneurons received the weakest input from vM1. In a representative SST interneuron, photo-stimulation elicited very small EPSCs, followed by a pronounced inhibitory postsynaptic current (IPSC; Fig. 1e). In contrast, the same photo-stimulation evoked substantially larger EPSCs in a neighboring pyramidal neuron (SST, −15.20 ± 2.00 pA; pyramidal, −137.89 ± 9.03 pA; $P < 0.001$, Mann-Whitney U test; Fig. 1e). We did not detect IPSCs in the pyramidal neuron. Under current-clamp mode, activation of vM1 inputs hyperpolarized the SST interneuron, but depolarized the nearby pyramidal neuron (SST, −1.31 ± 0.63 mV; pyramidal, 4.77 ± 0.27 mV; $P < 0.001$, Mann-Whitney U test; Fig. 1e). On average, photo-stimulation–evoked ESPCs in SST interneurons were significantly smaller than in pyramidal neurons (SST to pyramidal ratio, 0.12 ± 0.10, $P < 0.001$, Wilcoxon signed-rank test; Fig. 1f). Of 13 SST interneurons, we recorded reliable IPSCs following EPSCs from four SST interneurons, detected only small EPSCs in another four interneurons and failed to detect a response in the rest of the SST interneurons ($n = 5$), despite clear responses in the nearby pyramidal neuron. Other than SST interneurons, we observed sequences of EPSCs and IPSCs in only 2 of 51 pyramidal neurons. The fact that IPSCs always followed EPSCs strongly suggests that the IPSCs are triggered in a feedforward fashion by the same population of excitatory axons, that is, by the vM1 excitation of GABAergic interneurons in S1.

In contrast with all of the other cell types examined, SST interneurons showed facilitation to paired-pulse stimulation delivered at 5 Hz (paired-pulse ratio, 2.35 ± 1.11, $P = 0.03$, Wilcoxon signed-rank test). Facilitation became more notable in response to repetitive photo-stimulation (ten pulses) delivered at 40 Hz. Despite this, the vM1 input from to SST interneurons remained smaller than the input onto the pyramidal cell (Supplementary Fig. 3). We did not find differences in the latencies of the excitatory photo-stimulation evoked responses among the four groups of neurons (Supplementary Fig. 4a).

Together, these data indicate that the excitatory projection from vM1 most strongly recruits 5HT3aR interneurons compared with pyramidal cells or other interneurons. In contrast, vM1 provides minimal input to SST interneurons.

vM1 inputs most strongly drive VIP 5HT3aR neurons

Our data on the M1-to-S1 circuit suggest that that, among neurons in the superficial layers of S1 (that is, pyramidal neurons, and fast-spiking, SST and 5HT3aR interneurons), vM1 provides the strongest excitatory inputs to 5HT3aR interneurons. Although stimulation-evoked EPSCs of 5HT3aR interneurons were, on average, larger than those of other neuronal types, the range of normalized EPSCs in this class had a broad distribution (Fig. 1f). Thus, we asked whether the strength of vM1 input correlates with the specific subtype of 5HT3aR interneurons. 5HT3aR interneurons can be classified into two subgroups based on the expression of the neuropeptide VIP[15,16,19]. VIP-positive interneurons account for up to 40% of the 5HT3aR interneuron population. The most frequently observed VIP interneurons are the bipolar or bitufted neurons with an irregular-spiking firing pattern. Many VIP-negative 5HT3aR interneurons are reelin-positive, somatostatin-negative neurons with a late-spiking firing pattern and neurogliaform morphology[15,16,19]. We identified VIP and non-VIP interneurons on the basis of their firing patterns, as described in our previous studies[15,19]. We found that, of the 5HT3aR population, VIP interneurons received significantly stronger inputs from vM1 compared with nearby pyramidal neurons (VIP to pyramidal ratio = 2.88 ± 1.12, $P < 0.001$, Wilcoxon signed-rank test; Fig. 2). However, we found that EPSCs recorded from non-VIP 5HT3aR interneurons were similar to those recorded from pyramidal neurons (non-VIP to pyramidal ratio = 1.35 ± 0.45; $P = 0.51$, Wilcoxon signed-rank test; Fig. 2).

Given the dense arborizations of vM1 afferent axons in layer 1, we also examined whether the vM1 inputs to 5HT3aR interneurons were related to their laminar locations. Despite dense vM1 axons in layer 1, we did not find a relationship between the depth of 5HT3aR interneurons and responses to photo-stimulation (linear correlation: non-VIP, $r^2 = 0.078$; VIP, $r^2 = 0.001$; Fig. 2h). Our previous immunostaining data[15,19] and the visualization of VIP interneurons in a *Vip-cre* mouse crossed with a tdTomato-reporter line indicate that the somata of VIP interneurons are rarely observed in layer 1 and start to appear at the border between layer 1 and 2 (Supplementary Fig. 5). Although there were no somata of VIP interneurons in L1, their dendrites extended fully into L1 (Supplementary Fig. 5). Together, our results suggest that, of the 5HT3aR interneurons, VIP interneurons are most strongly excited by vM1 inputs.

We next compared local and long-range excitatory inputs (from vM1) to VIP interneurons. We simultaneously recorded EPSPs from pyramidal cells and either fast-spiking interneurons (*Pvalb-cre; tdTomato*) or VIP interneurons (*Vip-cre; tdTomato*) evoked by local electrical stimulation in layer 2/3 (Supplementary Fig. 6). We found that, on average, local electrical stimulation depolarized VIP interneurons about 40% less than pyramidal neurons (VIP to pyramidal ratio = 0.61 ± 0.12; $P = 0.02$, Wilcoxon signed-rank test; Supplementary Fig. 6). In contrast, local stimulation depolarized fast-spiking interneurons five times more strongly than pyramidal neurons (fast spiking to pyramidal ratio = 4.97 ± 0.64; $P = 0.02$, Wilcoxon signed-rank test; Supplementary Fig. 6)[26]. These results, together with the observed responses to the long-range inputs from vM1, provide evidence that local- and long-range excitatory inputs differentially recruit distinct types of GABAergic interneurons. Long-range vM1 excitatory inputs preferentially recruit VIP interneurons,

whereas local excitatory inputs strongly recruit fast-spiking interneurons in S1 superficial layers.

VIP interneurons preferentially inhibit SST interneurons

To understand how the strong recruitment of VIP interneurons by vM1 inputs affects the S1 network, we examined the functional output connectivity of VIP interneurons in S1. Anatomical studies have suggested that VIP interneurons preferentially target other types of interneurons[27,28]. To examine the functional connectivity of VIP interneurons, we recorded from pyramidal neurons, fast-spiking interneurons and SST interneurons while selectively photo-stimulating local VIP interneurons using a *Vip-cre* mouse line in conjunction with Cre-dependent expression of ChR2 as described above (Fig. 3). We limited the expression of ChR2 to just the VIP neurons in superficial layers (Supplementary Fig. 5).

We simultaneously recorded IPSCs from a fast-spiking interneuron and a nearby pyramidal neuron while photo-activating VIP interneurons in a *Vip-cre* B13 mouse. To isolate IPSCs, we used a cesium-based internal pipette solution under voltage-clamp mode while recording at the AMPA receptor reversal potential (0 mV). Photo-stimulation–evoked IPSCs in the pyramidal neuron were significantly larger than those in the fast-spiking neuron (pyramidal, 92.81 ± 11.87 pA; fast-spiking, 61.48 ± 9.67 pA, $P = 0.04$, Mann-Whitney U test; Fig. 3b). On average, the amplitude of IPSCs and the total inhibitory charge recorded from fast-spiking interneurons were about 35% and 85% less, respectively, than those in the simultaneously recorded pyramidal neurons (fast spiking to pyramidal ratio: amplitude = 0.66 ± 0.26, $P = 0.02$; charge = 0.16 ± 0.08, $P < 0.001$; Wilcoxon signed-rank test; Fig. 3d–f).

We also recorded from pairs of SST interneurons and pyramidal neurons in *Vip-cre* GIN mice. In contrast with fast-spiking interneurons, photo-stimulation of VIP interneurons generated IPSCs more than fourfold larger in a SST interneuron than in the simultaneously recorded pyramidal neuron (pyramidal, 111.40 ± 6.11 pA; SST, 440.81 ± 6.96 pA; $P < 0.001$, Mann-Whitney U test; Fig. 3c). As a population, VIP interneurons provided significantly larger inhibition to SST interneurons than to pyramidal neurons (SST to pyramidal ratio: amplitude = 5.06 ± 2.45, $P = 0.01$; charge = 6.44 ± 3.61, $P = 0.01$; Wilcoxon signed-rank test; Fig. 3d–f). IPSCs were completely blocked by GABAzine (data not shown), indicating that photo-stimulation evoked GABA release from VIP interneurons. Latencies of photo-stimulation–evoked responses from these three groups of neurons did not differ (pyramidal, 2.44 ± 0.18 ms; fast-spiking, 2.38 ± 0.26 ms; SST, 2.12 ± 0.15 ms; $P = 0.3$, Kruskal-Wallis test; Supplementary Fig. 4b).

These results indicate that, out of all of the excitatory and inhibitory elements in S1, VIP interneurons most strongly inhibit SST interneurons. The weakest connections of VIP interneurons were those with fast-spiking interneurons, the perisomatic targeting interneurons. The disynaptic feedforward inhibitory circuit created by the combination of the strong long-range vM1 excitatory inputs to VIP interneurons and the powerful local inhibitory connection of VIP interneurons with SST interneurons explains the pronounced delayed IPSCs recorded from SST interneurons in response to vM1 axon stimulation (Fig. 1e). To directly examine this, we optogenitcally silenced VIP interneurons while monitoring

inhibition in SST interneurons during photo-activation of vM1 axons (Fig. 4). We accomplished this by using *Vip-cre* GIN mice to selectively express the light-sensitive chloride pump (NpHR-eYFP) in VIP interneurons while using the eGFP expression to selectively record from SST interneurons (Fig. 4a). We also expressed ChR2-mCherry in vM1 to activate vM1 axons, as described above. Under these conditions, NpHR activation (590-nm photo-stimulation) strongly hyperpolarized NpHR-expressing VIP interneurons, whereas photo-stimulation (470 nm) of vM1 axons reliably depolarized and evoked spikes from VIP interneurons. When both NpHR and ChR2 were co-activated (590-nm and 470-nm photo-stimulation), NpHR activation sufficiently hyper-polarized VIP interneurons such that activation of vM1 inputs did not evoked spikes from the VIP interneurons (Fig. 4b). When VIP interneurons were not inhibited, photo-stimulation (470 nm) of vM1 axons evoked small EPSCs, followed by prominent IPSCs, in SST interneurons, as described above (Fig. 1e). Notably, optogenetic silencing of VIP interneurons strongly reduced the inhibitory current recorded from a SST interneuron during vM1 activation (470 nm + 590 nm, 0.27 ± 0.07 pC; 470 nm, 0.46 ± 0.06 pC; $P = 0.005$, Mann-Whitney U test; Fig. 4c). On average, inactivation of VIP interneurons during vM1 activation reduced the inhibition of SST interneurons by about 50% (470 nm + 590 nm to 470 nm ratio, 0.53 ± 0.09, $P = 0.008$, Wilcoxon signed-rank test; Fig. 4d). Together, these results provide direct evidence that excitatory inputs from vM1 recruit VIP interneurons and that these VIP interneurons in turn strongly inhibit SST interneurons, thereby establishing VIP interneuron–mediated disynaptic inhibition of SST interneurons during vM1 activation.

The activity of VIP interneurons increases during whisking

Our results indicate that S1-projecting vM1 pyramidal neurons strongly recruit VIP interneurons in S1 superficial layers and that VIP interneurons preferentially inhibit SST cells. These observations predict that the activity of VIP interneurons in S1 superficial layers will be increased and, conversely, that of SST interneurons will be decreased during voluntary whisking, that is, when the activity of vM1 is elevated[9,29–31].

To investigate this, we crossed *Vip-cre* mice with a tdTomato reporter line and a 5HT3aR^{eGFP} mouse (Fig. 5). This allowed us to visualize the 5HT3aR interneuron population and, more importantly, to distinguish VIP interneurons from non-VIP interneurons in the 5HT3aR interneuron population. We performed two-photon, targeted, loose-patch recordings from fluorescently labeled interneurons in S1 in awake behaving mice (Online Methods). Prior to *in vivo* recording, we habituated mice to the head-fixed condition under a microscope such that mice stayed quiet during the recording session, yet were fully awake and frequently showed whisking behavior[32]. Prior to the recordings, we mapped the barrel cortex with optical imaging of intrinsic signal induced by whisker stimulation. In parallel with recording spiking activity, we simultaneously recorded the electrocorticogram (ECoG) and whisker movement to monitor brain states and whisking behavior, respectively.

Under such recording conditions, we compared the firing rates during active whisking to those during awake non-whisking periods from the two different subtypes of 5HT3aR interneurons: VIP and non-VIP interneurons. An example VIP interneuron recorded at a

depth of 240 μm from the pia showed more than a threefold increase in its firing rate during active whisking, as compared with awake non-whisking periods (from 2.39 ± 0.42 Hz to 6.77 ± 1.63 Hz; Fig. 5b). In contrast with the VIP interneuron, a non-VIP interneuron (depth of 150 μm) recorded in the same mouse showed no changes in the firing rates between non-whisking and whisking periods (from 2.43 ± 0.45 Hz to 2.81 ± 0.52 Hz; Fig. 5c). The strong correlation between whisking behavior and the increased activity of VIP interneurons was also evident in the population data (whisking to non-whisking ratio = 3.3 ± 1.23, $P = 0.001$, Wilcoxon signed-rank test; Fig. 5e,h,i). Firing rates of non-VIP interneurons, however, did not differ in these two conditions (whisking to non-whisking ratio = 1.16 ± 0.28, $P = 0.94$, Wilcoxon signed-rank test; Fig. 5f,h,i). Spontaneous activity computed during non-whisking was similar between VIP interneurons and non-VIP interneurons (4.62 ± 3.20 Hz versus 5.15 ± 2.22 Hz, respectively; $P = 0.4$, Mann-Whitney U test). Consistent with previous studies[13,14,32], we also observed a correlation between whisking behavior and ECoG activity, with a predominant low-frequency component in the ECoG during non-whisking periods and the robust appearance of high-frequency ECoG during whisking (data not shown).

We also asked whether the activity of SST interneurons is inversely correlated with whisking behavior. We targeted SST interneurons using a *Sst-cre* mouse crossed with the tdTomato reporter line. A spontaneously active SST interneuron during non-whisking substantially decreased spiking activity once the mouse start to whisk (from 4.75 ± 0.97 Hz to 1.74 ± 0.34 Hz; Fig. 5d). We found, on average, more than a fourfold decrease in the firing rates of SST interneurons during active whisking as compared with non-whisking periods (whisking to non-whisking ratio = 0.24 ± 0.06, $P = 0.02$, Wilcoxon signed-rank test; Fig. 5g–i). This result is consistent with a previous finding that SST interneurons become hyperpolarized and exhibit reduced spiking activity during active whisking[14]. The differences in spiking behavior between VIP, non-VIP and SST interneurons did not depend on recording depth (Fig. 5j).

Given that vM1 activity is elevated during active whisking, these results suggest that vM1 directly recruits VIP interneurons in S1 in awake mice and that these neurons inhibit SST interneurons. To test causality between vM1 activity and the changes in the firing rates of VIP interneurons and SST interneurons in S1 during whisking, we inactivated vM1 using local injections of the sodium channel blocker tetrodotoxin (TTX; Fig. 6a). Spontaneously occurring, synchronized neuronal activity recorded from vM1 was completely abolished for several hours following TTX injections. Local field potentials (LFPs) recorded from S1, however, were not affected by TTX injection in vM1 (Fig. 6a). Following vM1 inactivation, the strong correlation between increased firing rates of VIP interneurons and whisking behavior was significantly reduced, suggesting that direct excitatory inputs from vM1 are responsible for the increased activity of VIP interneurons (whisking to non-whisking ratio = 1.42 ± 0.03, $P = 0.08$, Wilcoxon signed-rank test; Fig. 6b,d,e). Furthermore, we no longer observed the reduction of the activity of SST interneurons during whisking (whisking to non-whisking ratio = 0.98 ± 0.41, $P = 0.2$, Wilcoxon signed-rank test; Fig. 6c–e).

In summary, our results demonstrate a causal relationship between vM1 activity and the enhanced spiking rate of VIP interneurons in S1 superficial layers during whisking.

Moreover, we found that strong vM1 recruitment of VIP interneurons provides a powerful inhibition to SST interneurons, resulting in reduced spiking activity of these cells during whisking (Supplementary Fig. 7).

DISCUSSION

Here we characterized the synaptic targets of the axonal projections from vM1 in the mouse S1. We found that a specific subtype of GABAergic interneurons, the VIP-expressing irregular-spiking neurons, were the primary targets of vM1 projections. We also found that that SST-expressing interneurons were the main targets of VIP interneurons. Consistent with these findings, we observed that the *in vivo* activity of VIP interneurons in S1 was tightly correlated with voluntary whisking behavior when the overall activity of vM1 was elevated[9,29–31]. Furthermore, we found that vM1 activity was required to produce the increased firing rate of VIP interneurons. These findings suggest an underlying circuit mechanism that can explain the observed hyperpolarization and silencing of SST interneurons during whisking (Fig. 5)[13,14]. Consistent with this conclusion, inactivation of vM1 suppressed the silencing of SST interneurons during whisking. Together, our results describe a previously unknown disinhibitory circuit by which signals from motor cortex influence information processing in sensory cortex.

VIP neurons are a subtype of a family of interneurons that is characterized by the expression of 5HT3a receptors. Previously, we found that 5HT3aR interneurons account for ~30% of the GABAergic neurons in S1 and that, together with the interneurons expressing PV and SST, these can account for nearly all GABAergic neurons in the cortex[15,16]. Notably, 5HT3aR interneurons are enriched in superficial or associative layers, where they represent the most abundant GABAergic interneuron population. However, the physiological function of this group of interneurons has largely remained unknown. One study reported that some non–fast-spiking GABAergic interneurons increased their activity during whisking[13], but the interneuron subtype that these non–fast-spiking interneurons correspond to was not identified. Some of the observed non–fast-spiking GABArgic interneurons were presumably VIP interneurons, particularly those whose activity increases during whisking.

Superficial cortical layers are the main targets of interareal cortical communication. In primary sensory cortex they are the layers in which sensory information from layer 4, the thalamic recipient zone, is integrated with information from other columns and other cortical areas. Specifically, in S1 the densest projection of vM1 axons is found in L1 (refs. 2–5). The enrichment of 5HT3aR interneurons in superficial layers suggests that these interneurons may be important in mediating interareal cortical interactions and thereby contribute to context-dependent sensory processing. The finding that VIP interneurons are the main recipients in S1 of vM1 activity supports this hypothesis.

Although vM1 activity is necessary for increased activity of VIP interneurons, a trend in the same direction as that observed when vM1 was intact was still seen during M1 inactivation (Fig. 6). It is therefore possible that other factors, such as changes in the levels of neuromodulators, contribute to the activity of VIP interneurons during whisking.

Previous models of the mechanism by which vM1 activity influences S1 function have usually implied that vM1 effects are mediated by direct connections between vM1 axons and pyramidal cells in S1[9,10]. Our results suggest that interneurons are important and, specifically, that changes in the activity of S1 pyramidal cells depend on the feed-forward inhibition of the SST interneurons by VIP interneurons[13,14]. Given that SST interneurons primarily target the distal dendrites of pyramidal cells, our results suggest that a key effect of motor-sensory communication in S1 is the disinhibition of the distal dendrites of pyramidal cells. How does this disynaptic disinhibitory circuit mediate the effect of motor signals on the activity of S1? A hypothesis is suggested by recent findings on the effects of whisker movements on the activity of pyramidal cells in S1 together with what is known about the effects of SST interneurons on pyramidal cell activity. A recent study[10] found that the interaction between whisker sensory input and vM1 activity during the performance of an object localization task promotes large Ca^{2+} regenerative responses in the apical tuft dendrites of pyramidal cells in S1. On the other hand, SST interneurons have been shown to control the generation of Ca^{2+} regenerative activity in the distal dendrites of pyramidal cells[33–35]. Thus, the circuit unraveled in this study provides a mechanism to explain the generation of Ca^{2+} regenerative potentials during active sensing via the vM1-mediated feedforward inhibition of the SST interneurons by VIP interneurons. Ca^{2+} regenerative responses initiated in the distal dendrites of pyramidal neurons are known to promote burst spiking[33–36]. Bursts are more reliably transmitted across synapses than single spikes[37], and consistent with a role of SST in controlling burst spiking, it has been shown that silencing SST interneurons increases burst generation by pyramidal cells[14,33,35]. Thus, bursting might be the signal representing the coincident detection of sensory information and changes in whisker movements, which in turn could provide an amplification of certain sensory signals.

The axons of vM1 also branch in L5b/6 of S1. Increased vM1 activity enhances the activity of S1 L5b/6 pyramidal neurons[8,38], suggesting direct inputs from vM1. The disinhibitory circuit that we observed for L2/3 pyramidal neurons may also occur on the distal dendrites of L5b pyramidal neurons. How this modulation interacts with the actions of vM1 axons in L5b to control the activity of these neurons will need to be addressed in the future.

In addition to the projection from motor cortex, other cortical areas also project to S1. For example, the axons from the secondary somatosensory cortex (S2) reside for the most part in the same layers of S1 as the vM1 projections[2,39]. Furthermore, subcortical areas, such as the intralaminar and midline thalamic nuclei and the posteriomedial thalamic nucleus, also preferentially target the superficial layers[11,40–42]. Functionally, these nonspecific thalamic and higher order (association) nuclei are known to be involved in arousal and alertness[43,44] and serve as an interface between sensory and motor function in the whisker-to-barrel system[7,45,46] (but see ref. 47). A recent study found that neurogliaform cells, a subtype of non-VIP 5HT3aR interneurons, in prefrontal cortex are targets of inputs from midline thalamic nuclei[48]. Together with our results, these observations suggest that strong engagement of subtypes of 5HTaR interneurons might a general principle of circuit wiring in cortico-cortical and subcortical interactions.

Another recent study characterized the connectivity of two morphologically distinct subtypes of layer 1 interneurons[49]: L1 single-bouquet cells (SBCs) and elongated

neurogliaform cells. SBCs partly resemble the VIP interneurons characterized here, as both have a descending intracolumnar axon. Moreover, it was reported[49] that SBCs preferentially form unidirectional inhibitory connections on all subtypes of L2/3 interneurons and can therefore produce disinhibition of L5 pyramidal neurons in the same column. This raises the question of whether VIP interneurons correspond to the SBC neurons described previously[49]. On the basis of the following observations, we believe that SBCs and VIP interneurons are not the same cell type and that the disinhibitory circuit we observed is therefore distinct from the one described previously[49]. Specifically, according to the previous study[49], SBC interneurons are a prominent L1 interneuron. However, although the dendrites of VIP interneurons extended fully into layer 1 (Supplementary Fig. 5), VIP interneuron somas are rarely observed in this layer[15]. Furthermore, SBC cells and VIP interneurons appeared to have different output connectivity. According to the previous study[49], SBC cells connect to all interneuron subtypes in L2/3 and not to pyramidal cells. Furthermore, that study[49] found that the connection probability between SBCs and SST interneurons was the lowest for all supragranular interneurons. However, we observed small connectivity to all neurons, including pyramidal cells, but substantially stronger connectivity specifically to SST interneurons.

It has been suggested that the large diversity of GABAergic interneurons contributes to the ability of cortical circuits to perform a broad range of complex computations[50]. Our results provide further evidence that different types of GABAergic interneurons interact to modulate cortical circuits during different contextual and behavioral states.

ONLINE METHODS

Transgenic mice

We used the following transgenic mouse lines to target specific population of neurons: 5HT3aR-BAC^{eGFP} (BX663, Gensat) for 5HT3aR interneurons, B13, G42 (007677, Jackson) and *Pvalb-cre* (008069, Jackson) for PV interneurons, *Vip-cre* (008069, Jackson) for VIP interneurons, GIN (003718, Jackson), X94 (006334, Jackson) and *Sst-cre* (013044, Jackson) for SST interneurons, and *Emx1-cre* (005628, Jackson) for pyramidal neurons. All procedures were carried out in accordance with the US National Institutes of Health Guide for the Care and Use of Laboratory Animals and with the approval of the Institutional Animal Care and Use Committee of the New York University School of Medicine. The mice used in this study were from mixed backgrounds that included C57BL/6, CB6 and Swiss-Webster. Heterozygous mice were used for experiments. Both male and female mice were used. Mice were group-housed in the vivarium under reversed light-dark (12 h and 12 h) conditions. After surgery, mice were housed individually. The mice used in this study had no previous history of drug administration, surgery or behavioral testing.

Stereotactic virus injection

Mice (postnatal day 18–22) were anesthetized with isoflurane (1.0–1.5% isoflurane (vol/vol) in 100% oxygen) and positioned in a stereotactic frame for virus injection. A small craniotomy was made to target neurons in S1 and vM1 (vM1, 0.5–1.5 mm anterior and 0.5–1.0 lateral to bregma; S1, 1.2–1.5 mm posterior and 3.0–3.5 mm lateral to bregma). Adeno-

associated virus (AAV) was used for the expression of ChR2-mCherry. AAV2/5 (EF1-dflox-hChR2(H134R)-mCherry, Penn Vector Core) was delivered through a small craniotomy (~150 μm in diameter) by a glass micropipette (6–12-μm inner diameter, back-filled with mineral oil) attached to an automated nanoliter injector (Drummond Nanoject). To target neurons in superficial layer of S1, a bolus of 0.03 μl of virus was injected at each 50-μm step from a depth of 250 to 100 μm below the surface at the rate of 0.03 μl min^{-1}. To target vM1 neurons, virus was injected sequentially from a depth of 1,000 to 100 μm from the cortical surface. The pipette was held in the final position for 5–10 min before being retracted from the brain. Mice's eyes were protected with ointment (Vetropolycin) during the surgery.

Immunohistochemistry

2–3 weeks after (wt/vol) virus injection, mice were fixed by transcardiac perfusion with 0.9% saline (wt/vol) containing heparin (1 unit ml^{-1}), followed by 30–50 ml of 0.1 M phosphate buffer (pH 7.4) containing 4% paraformaldehyde (wt/vol). Dissected brains were further fixed in the same fixative solution for 1 h at 4 °C and then placed in a 30% sucrose (wt/vol) solution at 4 °C for 24–48 h. Using a sliding microtome, 40-μm-thick frozen coronal sections were collected in 0.1 M phosphate-buffered saline (PBS). Sections were washed in PBS and then incubated in a blocking solution (10% normal goat serum (vol/vol), 1% BSA (vol/vol), 0.2% cold fish gelatin (vol/vol) and 0.2% Triton X-100 (vol/vol) in PBS) for 1 h at 20–23 °C. Sections were then incubated with primary antibodies (rabbit antibody to VIP, 1:500 dilution, AB982, Incstar) in a diluted (1:10) blocking solution overnight at 4 °C, washed in PBS four times for 5 min each, followed by 1 h of secondary antibody incubation at 20–23 °C and washed four times in PBS for 5 min each. Cy2-conjugated secondary antibodies (1:200, 200-222-037, Jackson ImmunoResearch) were used to visualize the signals. Sections were mounted in Vectashield medium containing 4,6-diamidino-2-phenylindole (DAPI; Vector Laboratory) for nuclear counterstaining. Fluorescent images were taken using a Zeiss LSM 510 META confocal microscope.

In vitro electrophysiology and photo-stimulation

Brain slices were prepared and visualized, and whole-cell recordings were performed as described previously[15]. Briefly, 2–3 weeks after viral injection, mice were anesthetized with pentobarbital (100 mg per kg body weight) and transcardially perfused with cold perfusion solution containing 242.0 mM sucrose, 2.5 mM KCl, 0.0 or 0.5 mM $CaCl_2$, 7.0 mM $MgCl_2$, 28.0 mM $NaHCO_3$, 1.25 mM NaH_2PO_4 and 10.0 mM glucose saturated with 95% O_2/5% CO_2. Coronal slices (300 μm) were made using Vibratome 1000 Plus (Vibratome) in the same solution. Slices were incubated at 35 °C for 30 min and kept at 20–23 °C for at least 30 min before recording.

Whole-cell recordings were performed in oxygenated artificial cerebro-spinal fluid containing 125 mM NaCl, 26 mM $NaHCO_3$, 2.5 mM KCl, 1.25 mM NaH_2PO_4, 2 mM $CaCl_2$, 2 mM $MgCl_2$ and 10 mM glucose. The artificial cerebro-spinal fluid was continuously equilibrated with 95% O_2 and 5% CO_2 throughout recording. For EPSP and EPSC recordings, glass pipettes (3–6 MΩ) were filled with internal solution containing 135 mM potassium gluconate, 4 mM KCl, 2 mM NaCl, 10 mM HEPES, 0.2 mM EGTA, 4 mM

ATP-Mg, 0.3 mM GTP-Tris, 1.4 mM phosphocreatine-Tris (pH 7.25, 280 mOsm) and 0.2% biocytin (wt/vol). For IPSC recordings, pipettes were filled with 130 mM cesium gluconate, 0.5 mM EGTA, 7 mM KCl, 10 mM HEPES, 4 mM Mg-ATP, 0.3 mM Na-GTP, 5 mM phosphocreatine, 5 mM QX-314 (pH 7.25 with CsOH) and 0.2% biocytin. Membrane potentials were not corrected for the liquid junction potential. Recordings were conducted at 30–33 °C. During patching, cell-attached seal resistances were >1 GΩ and series resistance after achieving whole-cell configuration was between 5 and 28 MΩ. A series of hyperpolarizing and depolarizing step currents were injected to measure intrinsic properties of each neuron. Data was collected using an Axopatch 200B and 2B amplifiers (Molecular Devices), sampled at 20 kHz and low-pass filtered at 5 kHz (Digidata 1322A, Molecular Devices). pCLAMP 9 software (Molecular Devices) was used for data acquisition, and analysis was performed using the Clampfit module of pCLAMP. To visualize the morphology of recorded neurons, slices were fixed for 1–2 h with 4% paraformaldehyde in PBS, rinsed with PBS, and incubated in a blocking solution (1% normal goat serum and 0.3% Triton X-100, pH 7.5, in PBS) for 2 h. After several washes with PBS, biocytin-filled neurons were stained using streptavidin-conjugated Alexa Fluor 555 (1:500 dilution, Invitrogen). Fluorescently labeled neurons were imaged and reconstructed using Zeiss LSM 510 META confocal microscope and Neurolucida software (MicroBrightField).

ChR2 and NpHR were excited with a 470- or 590-nm LED light source (Mightex), respectively. Collimated light from an LED was delivered through the epifluorescence pathway of Olympus BX61 microscope and fed into a 40× water-immersion objective. Photo-stimulation was delivered at 60-s intervals with the illumination intensity (2 mW) and duration (5 ms) controlled by a LED controller (Mightex).

Surgical procedure for head-fixed awake recordings

Mice (postnatal day 30–40) underwent aseptic surgeries under isoflurane anesthesia similar to virus injection procedure (see above). During surgical procedure, mice were kept on a heating pad (FHC) to maintain body temperature at 37 °C. A custom-built, T-shaped titanium headpost was mounted on the skull (overlaying the midline and the cerebellum) using cyanoacrylate glue (Vetbond) and subsequently covered by dental cement. Two screws were inserted in the skull above the left frontal and primary auditory cortex to secure dental cement. Two teflon-coated stainless steel wires (diameter = 0.1 mm, ~0.7 mm of a wire tip was exposed) were implanted to the left side of frontal cortex and to near secondary visual cortex for ECoG recording.

1 or 2 d after surgery, intrinsic imaging was performed to identify primary barrel cortex under isoflurane anesthesia[51]. Intrinsic imaging signals were obtained by measuring the difference between images acquired during stimulus and baseline periods. Difference image was calculated over 40 epochs with each epoch lasting for 13 s, including 4 s of whisker stimulation (at 10 Hz) and 9 s of baseline. Images were taken by a 14-bit CCD camera (Pixelfly USB, PCO) at 10 fps through the intact skull over the primary somatosensory cortex (using a 600 nm LED for illumination) to identify a cortical area associated with stimulation of a single whisker.

4–6 d after the initial surgery, each mouse had undergone a habituation to *in vivo* recording set-up with their heads fixed under a two-photon microscope[13,14]. The daily habituation training lasted for 5–8 d, until the mouse could stay in the *in vivo* recording set-up calmly for up to 2 h. A mouse was rewarded with sweetened water during and after training sessions. Mice were not water deprived.

Inactivation of vM1

The sodium channel blocker TTX (Tocris) was used to inactivate vM1. TTX (50 μM) and micro-Ruby (10%, vol/vol, Invitrogen), dissolved in saline (total 90-nl injection), were slowly injected to vM1 (1.1 mm lateral to the midline and 0.9 mm anterior to bregma) in the ipsilateral side of the S1 recording site using a nanoliter injector. The injections were made every 100 μm (15 nl for each injection site with speed of 15 nl per min) from 800 to 300 μm below pia. Mice were anesthetized during the injection procedure (see above). LFP recordings from vM1 and S1 were made before and after TTX injection to vM1 to confirm the TTX effect. After each *in vivo* targeted recording, LFP recordings from vM1 were carried out to ensure that vM1 was silence. The location of the vM1 injection site was confirmed with micro-Ruby.

In vivo electrophysiology

On the day of recording, under the light isoflurane anesthesia described above, a small craniotomy (<0.6 mm in diameter) was made over right side of barrel cortex, which was marked previously by intrinsic imaging. A small chamber was made out of dental cement to surround the craniotomy and covered by 1.5% agar dissolved in normal rat ringer (NRR) solution (135 mM NaCl, 5.4 mM KCl, 1.0 mM $MgCl_2$, 1.8 mM $CaCl_2$ and 5 mM HEPES, pH 7.2–7.4). A slit was made in the cranial dura just big enough for the entrance of a recording pipette. Recordings began 2 h after making the craniotomy to allow for the mouse to recover from anesthesia.

Targeted loose cell-attached recordings were performed under the guidance of two-photon imaging[52]. Pulled glass micropipettes (3–5 MΩ) were filled with the same internal pipette solution as for *in vitro* experiments (see above) supplemented with either Alexa Fluor 594 (5 μM, Invitrogen) to target GFP-positive neurons or Alexa Fluor 488 (5 μM, Invitrogen) to target tdTomato-positive neurons. Two-photon laser was tuned to 860 nm, which allowed excitation of both GFP/Alexa Fluor 488 and tdTomato/Alexa Fluor 594 fluorophores simultaneously. Loose patch recordings (40–120 MΩ) were performed in voltage-clamp mode using Axopatch 200B amplifier (Molecular Devices) sampled at 10 kHz and low-pass filtered at 5 kHz (Digidata 1322A; Molecular Devices). All recorded neurons were located from 50 μm to 250 μm below the cortical surface.

The ECoG signal was recorded using a differential amplifier (AC 1800, A-M system) bandpass filtered between 0.1 Hz and 10 kHz and digitized at 10 kHz using Digidata 1322A (Molecular Devices).

In vitro recording data analysis

To characterize the intrinsic membrane properties of neurons, hyperpolarizing and depolarizing current steps of 500-ms duration were applied in 10-pA increments at 0.125 Hz as described previously[15,19]. Two parameters were measured: resting membrane potential (V_{rest}), defined as the stable membrane potential reached after break in with no holding current applied, and input resistance (R_m), defined as the slope of the linear regression of the steady-state *I*-*V* curve. We used the value of the spike threshold as the EPSP amplitude for the neurons that elicited spikes in Figure 1.

Whisking behavior data analysis

To better quantify whisker movement, some whiskers were trimmed right before a recording session, leaving two rows of whiskers. To film whisking behavior, we used a high-speed camera (120 fps, Basler, SCA640) combined with an infrared illumination (630-nm LED). Custom-written image analysis script in Matlab (Mathworks) was used to measure overall whisker movement. To quantify periods of active whisking, we computed a series of spatial derivatives between successive pairs of video frames, generating a series of two-dimensional motion estimates. We then chose an image motion threshold that best discriminated periods of whisking from periods of rest. The motion estimates for each experiment were subsequently resampled to 20 Hz for graphical display.

In vivo recording data analysis

Custom-written Matlab (Mathworks) scripts were used to analyze electrophysiology data. For cell-attached recordings, spikes were detected on the basis of their amplitude (at least threefold larger than s.d. of baseline noise). Spikes were assigned to whisking or non-whisking periods on the basis of the whisking activity (see above), but barring any other body movements. Spectrograms of the ECoG were generated using the Matlab with a 1-s sliding window.

Data is presented throughout as mean ± s.d. except where otherwise noted. Unless stated otherwise, all statistical comparisons are non-parametric (two-sided). Specific statistical analyses are notified in the results. Data collection and analysis were not performed blind to the conditions of the experiments. Data were collected and processed without randomization. No statistical methods were used to pre-determine sample sizes.

Statistical analyses

Data is presented throughout as mean ± s.d. except where otherwise noted. Unless stated otherwise, all statistical comparisons are non-parametric (two-sided). Specific statistical analyses are notified in the results. Data collection and analysis were not performed blind to the conditions of the experiments. Data were collected and processed without randomization. No statistical methods were used to pre-determine sample sizes.

Supplementary Material

Refer to Web version on PubMed Central for supplementary material.

Acknowledgments

We thank all of the members of the Rudy and Fishell laboratories for helpful discussions. We thank K. Deisseroth (Stanford University) for DIO-ChR2-mCherry plasmids, Z. Talbot for help with intrinsic imaging and setting-up a camera for whisking behavior, and E. Merriam for advice on *in vivo* data analysis. This work was supported by grants from the US National Institutes of Health (R01 NS30989 and P01 NS074972 to B.R., MH071679 and P01 NS074972 to G.F., and 1F32NS076316 to S.L.). I.K. was supported by Epilepsy Foundation grant 260691.

References

1. Jones EG, Wise SP. Size, laminar and columnar distribution of efferent cells in the sensory-motor cortex of monkeys. J Comp Neurol. 1977; 175:391–438. [PubMed: 410849]
2. White EL, DeAmicis RA. Afferent and efferent projections of the region in mouse SmL cortex which contains the posteromedial barrel subfield. J Comp Neurol. 1977; 175:455–482. [PubMed: 915034]
3. Porter LL, White EL. Afferent and efferent pathways of the vibrissal region of primary motor cortex in the mouse. J Comp Neurol. 1983; 214:279–289. [PubMed: 6853758]
4. Donoghue JP, Parham C. Afferent connections of the lateral agranular field of the rat motor cortex. J Comp Neurol. 1983; 217:390–404. [PubMed: 6886060]
5. Veinante P, Deschênes M. Single-cell study of motor cortex projections to the barrel field in rats. J Comp Neurol. 2003; 464:98–103. [PubMed: 12866130]
6. Kleinfeld D, Ahissar E, Diamond ME. Active sensation: insights from the rodent vibrissa sensorimotor system. Curr Opin Neurobiol. 2006; 16:435–444. [PubMed: 16837190]
7. Diamond ME, von Heimendahl M, Knutsen PM, Kleinfeld D, Ahissar E. 'Where' and 'what' in the whisker sensorimotor system. Nat Rev Neurosci. 2008; 9:601–612. [PubMed: 18641667]
8. Lee S, Carvell GE, Simons DJ. Motor modulation of afferent somatosensory circuits. Nat Neurosci. 2008; 11:1430–1438. [PubMed: 19011625]
9. Petreanu L, et al. Activity in motor-sensory projections reveals distributed coding in somatosensation. Nature. 2012; 489:299–303. [PubMed: 22922646]
10. Xu NL, et al. Nonlinear dendritic integration of sensory and motor input during an active sensing task. Nature. 2012; 492:247–251. [PubMed: 23143335]
11. Petreanu L, Mao T, Sternson SM, Svoboda K. The subcellular organization of neocortical excitatory connections. Nature. 2009; 457:1142–1145. [PubMed: 19151697]
12. Hooks BM, et al. Laminar analysis of excitatory local circuits in vibrissal motor and sensory cortical areas. PLoS Biol. 2011; 9:e1000572. [PubMed: 21245906]
13. Gentet LJ, Avermann M, Matyas F, Staiger JF, Petersen CC. Membrane potential dynamics of GABAergic neurons in the barrel cortex of behaving mice. Neuron. 2010; 65:422–435. [PubMed: 20159454]
14. Gentet LJ, et al. Unique functional properties of somatostatin-expressing GABAergic neurons in mouse barrel cortex. Nat Neurosci. 2012; 15:607–612. [PubMed: 22366760]
15. Lee S, Hjerling-Leffler J, Zagha E, Fishell G, Rudy B. The largest group of superficial neocortical GABAergic interneurons expresses ionotropic serotonin receptors. J Neurosci. 2010; 30:16796–16808. [PubMed: 21159951]
16. Rudy B, Fishell G, Lee S, Hjerling-Leffler J. Three groups of interneurons account for nearly 100% of neocortical GABAergic neurons. Dev Neurobiol. 2011; 71:45–61. [PubMed: 21154909]
17. Kawaguchi Y. Physiological subgroups of nonpyramidal cells with specific morphological characteristics in layer II/III of rat frontal cortex. J Neurosci. 1995; 15:2638–2655. [PubMed: 7722619]
18. Tamás G, Lorincz A, Simon A, Szabadics J. Identified sources and targets of slow inhibition in the neocortex. Science. 2003; 299:1902–1905. [PubMed: 12649485]
19. Miyoshi G, et al. Genetic fate mapping reveals that the caudal ganglionic eminence produces a large and diverse population of superficial cortical interneurons. J Neurosci. 2010; 30:1582–1594. [PubMed: 20130169]

20. Porter JT, et al. Properties of bipolar VIPergic interneurons and their excitation by pyramidal neurons in the rat neocortex. Eur J Neurosci. 1998; 10:3617–3628. [PubMed: 9875341]
21. Chan CH, et al. Emx1 is a marker for pyramidal neurons of the cerebral cortex. Cereb Cortex. 2001; 11:1191–1198. [PubMed: 11709490]
22. Tsai HC, et al. Phasic firing in dopaminergic neurons is sufficient for behavioral conditioning. Science. 2009; 324:1080–1084. [PubMed: 19389999]
23. Dantzker JL, Callaway EM. Laminar sources of synaptic input to cortical inhibitory interneurons and pyramidal neurons. Nat Neurosci. 2000; 3:701–707. [PubMed: 10862703]
24. Oliva AA Jr, Jiang M, Lam T, Smith KL, Swann JW. Novel hippocampal interneuronal subtypes identified using transgenic mice that express green fluorescent protein in GABAergic interneurons. J Neurosci. 2000; 20:3354–3368. [PubMed: 10777798]
25. Ma Y, Hu H, Berrebi AS, Mathers PH, Agmon A. Distinct subtypes of somatostatin containing neocortical interneurons revealed in transgenic mice. J Neurosci. 2006; 26:5069–5082. [PubMed: 16687498]
26. Mateo C, et al. *In vivo* optogenetic stimulation of neocortical excitatory neurons drives brain-state-dependent inhibition. Curr Biol. 2011; 21:1593–1602. [PubMed: 21945274]
27. Gonchar Y, Burkhalter A. Differential subcellular localization of forward and feedback interareal inputs to parvalbumin expressing GABAergic neurons in rat visual cortex. J Comp Neurol. 1999; 406:346–360. [PubMed: 10102500]
28. Dávid C, Schleicher A, Zuschratter W, Staiger JF. The innervation of parvalbumin containing interneurons by VIP-immunopositive interneurons in the primary somatosensory cortex of the adult rat. Eur J Neurosci. 2007; 25:2329–2340. [PubMed: 17445231]
29. Carvell GE, Miller SA, Simons DJ. The relationship of vibrissal motor cortex unit activity to whisking in the awake rat. Somatosens Mot Res. 1996; 13:115–127. [PubMed: 8844960]
30. Huber D, et al. Multiple dynamic representations in the motor cortex during sensorimotor learning. Nature. 2012; 484:473–478. [PubMed: 22538608]
31. Friedman WA, Zeigler HP, Keller A. Vibrissae motor cortex unit activity during whisking. J Neurophysiol. 2012; 107:551–563. [PubMed: 21994257]
32. Crochet S, Petersen CC. Correlating whisker behavior with membrane potential in barrel cortex of awake mice. Nat Neurosci. 2006; 9:608–610. [PubMed: 16617340]
33. Murayama M, et al. Dendritic encoding of sensory stimuli controlled by deep cortical interneurons. Nature. 2009; 457:1137–1141. [PubMed: 19151696]
34. Larkum ME, Zhu JJ, Sakmann B. A new cellular mechanism for coupling inputs arriving at different cortical layers. Nature. 1999; 398:338–341. [PubMed: 10192334]
35. Larkum M. A cellular mechanism for cortical associations: an organizing principle for the cerebral cortex. Trends Neurosci. 2013; 36:141–151. [PubMed: 23273272]
36. Williams SR, Stuart GJ. Mechanisms and consequences of action potential burst firing in rat neocortical pyramidal neurons. J Physiol (Lond). 1999; 521:467–482. [PubMed: 10581316]
37. Lisman JE. Bursts as a unit of neural information: making unreliable synapses reliable. Trends Neurosci. 1997; 20:38–43. [PubMed: 9004418]
38. Kinnischtzke AK, Simons DJ, Fanselow EE. Motor cortex broadly engages excitatory and inhibitory neurons in somatosensory barrel cortex. Cereb Cortex. Mar 31.2013 published online. 10.1093/cercor/bht085
39. Fabri M, Burton H. Ipsilateral cortical connections of primary somatic sensory cortex in rats. J Comp Neurol. 1991; 311:405–424. [PubMed: 1720147]
40. Herkenham M. Laminar organization of thalamic projections to the rat neocortex. Science. 1980; 207:532–535. [PubMed: 7352263]
41. Wimmer VC, Bruno RM, de Kock CP, Kuner T, Sakmann B. Dimensions of a projection column and architecture of VPM and POm axons in rat vibrissal cortex. Cereb Cortex. 2010; 20:2265–2276. [PubMed: 20453248]
42. Ohno S, et al. A morphological analysis of thalamocortical axon fibers of rat posterior thalamic nuclei: a single neuron tracing study with viral vectors. Cereb Cortex. 2012; 22:2840–2857. [PubMed: 22190433]

43. Van der Werf YD, Witter MP, Groenewegen HJ. The intralaminar and midline nuclei of the thalamus. Anatomical and functional evidence for participation in processes of arousal and awareness. Brain Res Brain Res Rev. 2002; 39:107–140. [PubMed: 12423763]
44. Shirvalkar P, Seth M, Schiff ND, Herrera DG. Cognitive enhancement with central thalamic electrical stimulation. Proc Natl Acad Sci USA. 2006; 103:17007–17012. [PubMed: 17065322]
45. Yu C, Derdikman D, Haidarliu S, Ahissar E. Parallel thalamic pathways for whisking and touch signals in the rat. PLoS Biol. 2006; 4:e124. [PubMed: 16605304]
46. Kleinfeld D, Ahissar E, Diamond ME. Active sensation: insights from the rodent vibrissa sensorimotor system. Curr Opin Neurobiol. 2006; 16:435–444. [PubMed: 16837190]
47. Masri R, Bezdudnaya T, Trageser JC, Keller A. Encoding of stimulus frequency and sensor motion in the posterior medial thalamic nucleus. J Neurophysiol. 2008; 100:681–689. [PubMed: 18234976]
48. Cruikshank SJ. Thalamic control of layer 1 circuits in prefrontal cortex. J Neurosci. 2012; 32:17813–17823. [PubMed: 23223300]
49. Jiang X, Wang G, Lee AJ, Stornetta RL, Zhu JJ. The organization of two new cortical interneuronal circuits. Nat Neurosci. 2013; 16:210–218. [PubMed: 23313910]
50. Klausberger T, Somogyi P. Neuronal diversity and temporal dynamics: the unity of hippocampal circuit operations. Science. 2008; 321:53–57. [PubMed: 18599766]
51. Chen-Bee CH, et al. Visualizing and quantifying evoked cortical activity assessed with intrinsic signal imaging. J Neurosci Methods. 2000; 97:157–173. [PubMed: 10788670]
52. Komai S, Denk W, Osten P, Brecht M, Margrie TW. Two-photon targeted patching (TPTP) *in vivo*. Nat Protoc. 2006; 1:647–652. [PubMed: 17406293]

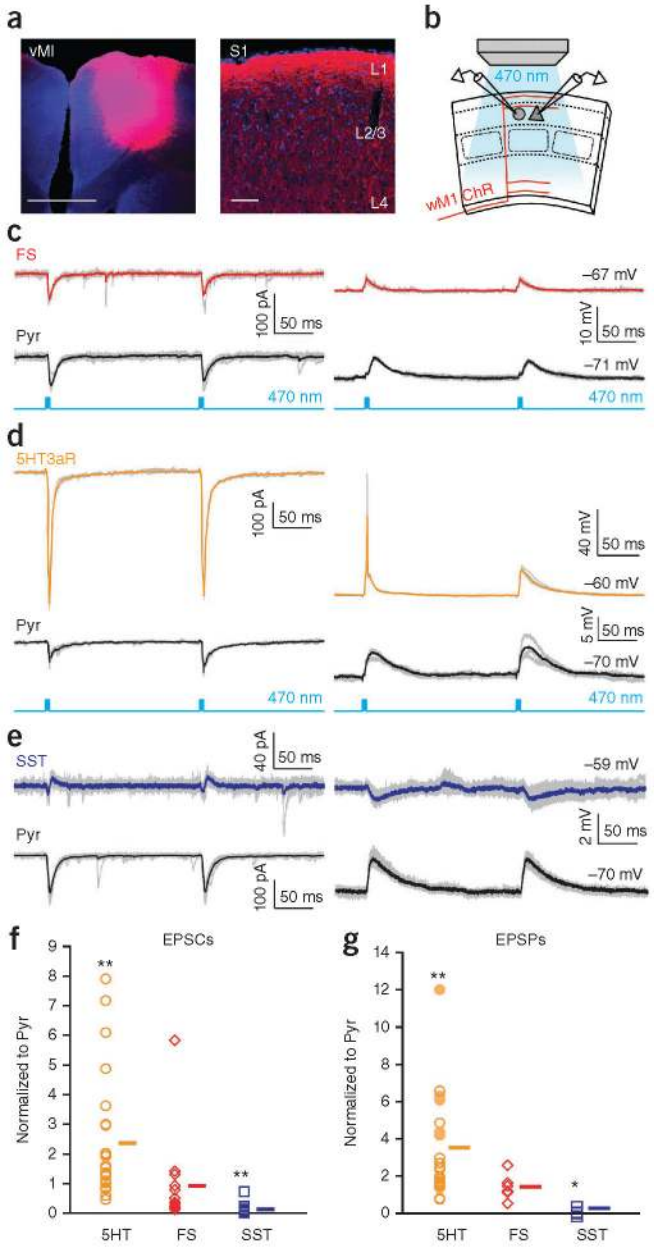

Figure 1.

Long-range excitatory inputs from vM1 to different types of neurons in the superficial layers of S1. (**a**) Expression of ChR2-mCherry in vM1 pyramidal neurons. Left, expression of ChR2 in vM1 after injection of AAV-DIO-ChR2-mCherry to vM1 in *Emx1-cre* mice. Scale bar represents 500 μm. Right, axons of vM1 pyramidal neurons innervating S1 expressed ChR2-mCherry. Scale bar represents 100 μm. Note the strong expression of ChR2-mCherry in layers 1 and 2 in S1 (blue, DAPI). (**b**) Schematic of slice recording configuration. Red lines indicate the innervation patterns of vM1 axons. A specific interneuron type was simultaneously recorded with a nearby pyramidal neuron. (**c**–**e**) Photo-stimulation–evoked synaptic currents (left) and voltage responses (right) recorded in a fast-spiking (FS) interneuron and a pyramidal (Pyr) neuron (**c**), a 5HT3aR interneuron and a pyramidal

neuron (**d**), and a SST interneuron and a pyramidal neuron (**e**). Gray traces represent individual sweeps and solid colored traces represent the average (red for fast spiking, orange for 5HT3aR, blue for SST and black for pyramidal neurons). Evoked synaptic currents were recorded at −70 mV in voltage-clamp mode. Voltage responses were recorded at the resting membrane potential (V_{rest}, indicated next to the voltage traces) under current-clamp mode. Light blue traces indicate photo-stimulation (LED, 470 nm, 5 ms) delivered at 5 Hz. (**f**,**g**) EPSCs (**f**) and EPSPs (**g**) of 5HT3aR (5HT), fast-spiking and SST interneurons normalized to simultaneously recorded nearby pyramidal neurons (normalized EPSCs: 5HT3aR, 25 cells, 18 slices, 8 mice, $P < 0.001$; fast spiking, 13 cells, 8 slices, 4 mice, $P = 0.1$; SST, 13 cells, 9 slices, 4 mice, $P < 0.001$; normalized EPSPs: 5HT3aR, 21 cells, 17 slices, 8 mice, $P < 0.001$; fast spiking, 6 cells, 4 slices, 2 mice, $P = 0.18$; SST, 6 cells, 4 slices, 2 mice, $P = 0.01$). Statistical significance was computed using Wilcoxon signed-rank test; $^{*}P < 0.05$, $^{**}P < 0.005$. Bars indicate mean.

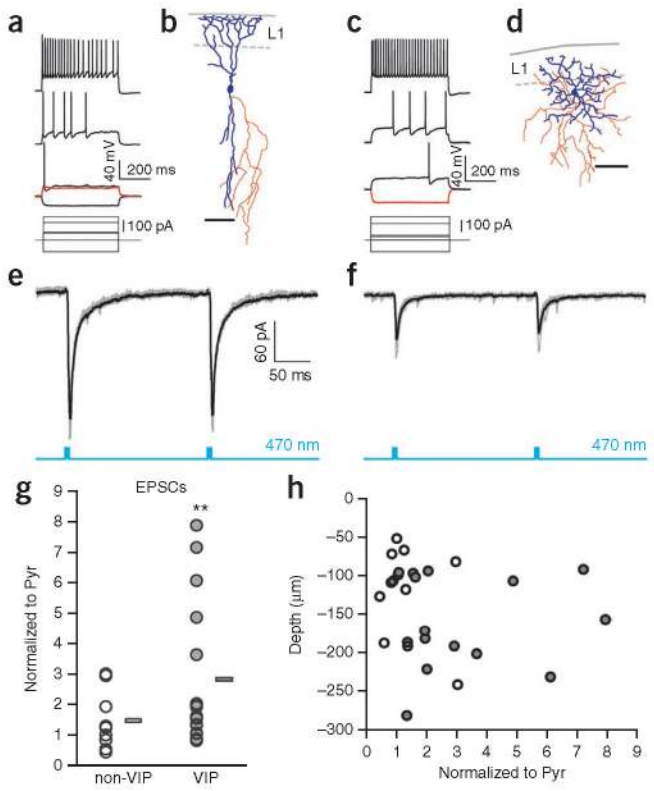

Figure 2.

VIP interneurons receive the strongest input from vM1. (**a**,**c**) Representative firing patterns of an irregular spiking neuron (**a**, VIP-positive 5HT3aR interneuron) and a late spiking neuron (**c**, non-VIP, 5HT3aR interneuron) produced by increasing step current injections (500 ms) in current-clamp mode. (**b**,**d**) Examples of morphologies of the irregular-spiking (**b**) and late-spiking (**d**) interneurons reconstructed using Neurolucida tracing. Dendrite and soma are shown in blue and axon in red. Scale bars represent 100 µm. (**e**,**f**) EPSCs evoked by photo-stimulation of vM1 axons, recorded in the irregular-spiking neuron (**e**) and the late-spiking neuron (**f**). Blue traces indicate photo-stimulation (LED, 470 nm, 5 ms) delivered at 5 Hz. (**g**) VIP interneurons received significantly stronger vM1 inputs compared with non-VIP interneurons in the 5HT3aR population. EPSCs of VIP and non-VIP interneurons were normalized to simultaneously recorded nearby pyramidal neurons. Bars indicate mean value (VIP interneurons: 15 cells, 12 slices, 8 mice, VIP to pyramidal ratio, $P < 0.001$; non-VIP interneurons: 10 cells, 7 slices, 6 mice, non-VIP to pyramidal ratio, $P = 0.51$). $^{**}P < 0.005$, Wilcoxon signed-rank test. (**h**) We found no relationship between the recording depth (relative to pial surface) and the strength of the vM1 input. Recording depth is plotted against normalized EPSC. White circles represent non-VIP interneurons and gray circles represent VIP interneurons (correlation coefficient: non-VIP, $r^2 = 0.078$; VIP, $r^2 = 0.001$).

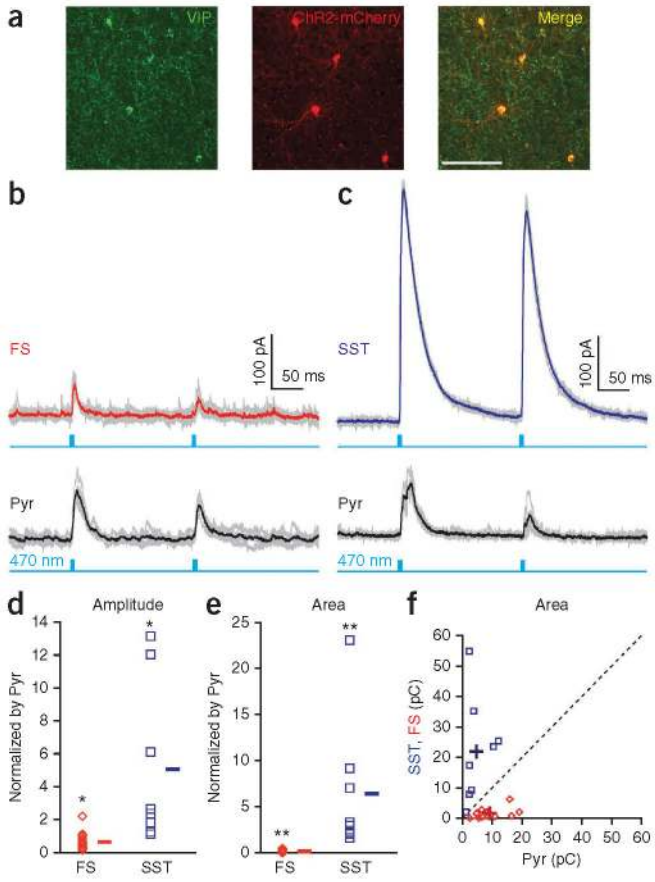

Figure 3.

VIP interneurons most strongly inhibit SST interneurons in S1 superficial layers. (**a**) Specific expression of ChR2-mCherry in VIP interneurons. ChR2-mCherry expression in *Vip-cre* mice was confined to VIP neurons. Antibody-stained VIP neurons (left) showed nearly 100% overlap (right) with neurons expressing ChR2-mCherry (middle). Scale bar represents 100 μm. (**b**) VIP interneurons provided weak inhibition to fast-spiking interneurons. Photo-stimulation–evoked inhibitory synaptic currents recorded in a fast-spiking interneuron and in a pyramidal neuron in the *Vip-cre* B13 mouse are shown. (**c**) VIP interneurons provided strong inhibition to SST interneurons. Photo-stimulation–evoked inhibitory synaptic currents in a SST interneuron and a simultaneously recorded pyramidal neuron in a *Vip-cre* GIN mouse are shown. Cesium-based internal pipette solution was used to record inhibitory currents at 0 mV in voltage-clamp mode. Gray traces indicate individual sweeps and colored traces indicate the average (red, fast spiking; blue, SST; black, pyramidal neurons). Light blue traces indicate photo-stimulation (LED, 470 nm, 5 ms) delivered at 5 Hz. (**d**,**e**) IPSC amplitude (**d**) and total charge (**e**) in fast-spiking (14 cells, 8 slices, 4 mice) and SST (8 cells, 5 slices, 3 mice) interneurons normalized to the corresponding values in simultaneously recorded nearby pyramidal neurons. *$P < 0.05$, **$P < 0.005$, Wilcoxon signed-rank test. (**f**) Photo-stimulation–evoked total IPSC charge in fast-spiking interneurons (red) and SST interneurons (blue) plotted against total IPSC charge in simultaneously recorded pyramidal neurons. Dashed line indicates unity. + indicates mean

(fast spiking to pyramidal ratio: amplitude, $P = 0.02$; charge, $P < 0.001$; SST to pyramidal ratio: amplitude, $P = 0.01$; charge, $P < 0.001$).

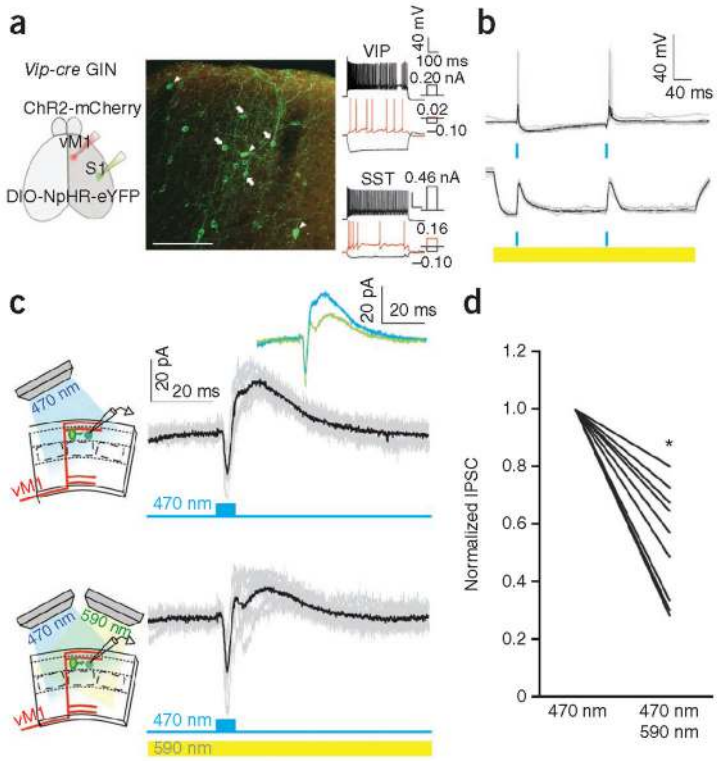

Figure 4.

VIP interneurons mediate disynaptic feedforward inhibition of SST interneurons following vM1 activation. (**a**) Specific expression of NpHR-eYFP in VIP interneurons. AAV-ChR2-mCherry was injected to vM1 and AAV-DIO-NpHR-eYFP in S1 of a *Vip-cre* GIN mouse (left). Middle, expression of NpHR-eYFP in VIP interneurons in S1. NpHR-eYFP–expressing VIP interneurons (arrow) were easily distinguishable from GIN neurons (arrowhead) as a result of the preferential labeling of the periphery of the cells resulting from membrane expression of eYFP in VIP interneurons. Note the mCherry-expressing vM1 axons in layer 1 of S1. Scale bar represents 100 μm. Right, firing patterns of a NpHR-eYFP–expressing VIP interneuron and a GIN interneuron. (**b**) Activation of NpHR reduced vM1 activation-evoked spikes from NpHR-expressing VIP interneurons. Photo-stimulation of vM1 axons (blue light, 470 nm) elicited reliable spikes from a VIP interneuron in S1 (top). Photo-stimulation (yellow light, 590 nm) of NpHR sufficiently hyperpolarized the VIP interneuron such that simultaneous photo-stimulation (blue light, 470 nm) of ChR2-expressing vM1 axons evoked only subthreshold EPSPs in the VIP interneuron (bottom). (**c**) VIP interneurons mediated disynaptic feedforward inhibition of SST interneurons during vM1 activation. Left, schematic of slice recording and photo-stimulation configuration. Right, evoked EPSCs followed by IPSCs recorded from a SST interneuron to blue light (top) and blue light combined with yellow light (bottom). Inset, overlay of averaged postsynaptic currents traces to blue light only (blue trace) and blue light combined with yellow light (green). Gray traces represent individual sweeps, and black traces show the average. Evoked synaptic currents were recorded at −55 mV in voltage-clamp mode. (**d**) Population data from **c**. Blue and yellow light stimulation–evoked total IPSC charge was normalized to blue light

only stimulation–evoked response in SST interneurons (9 cells, 6 slices, 3 mice; 470 nm + 590 nm to 470 nm ratio, charge $P = 0.008$). *$P < 0.05$, Wilcoxon signed-rank test.

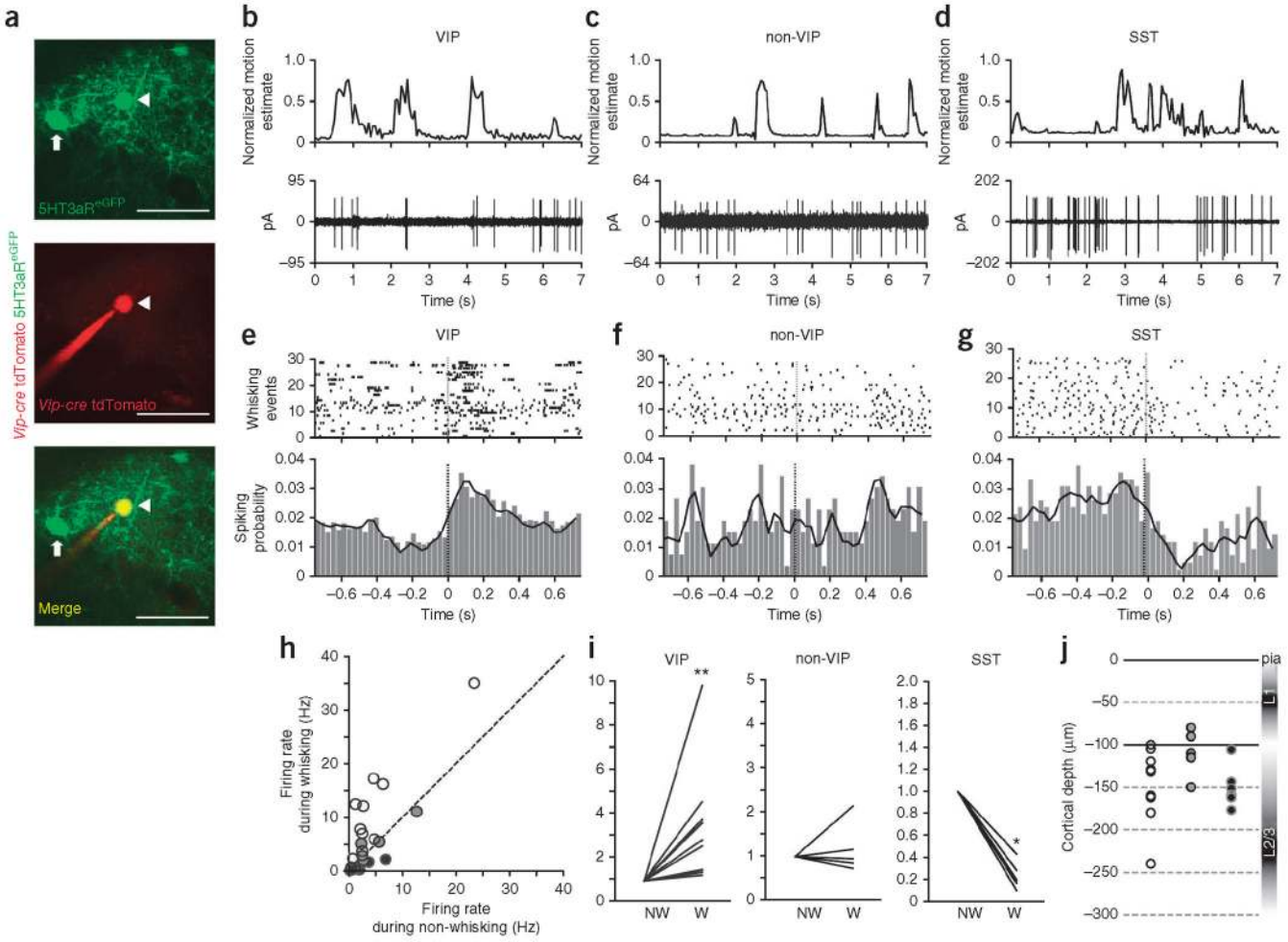

Figure 5.

Spiking activity of VIP interneurons and SST interneurons in superficial layers of S1 during active whisking. (**a**) Image of an eGFP-positive and tdTomato-positive cell targeted for cell-attached *in vivo* recording in a *Vip-cre* tdTomato 5HT3aR^{eGFP} mouse. Arrow points to an eGFP-positive, tdTomato-negative interneuron (non-VIP interneuron) and the arrowhead points to an eGFP-positive, tdTomato-positive interneuron (VIP interneuron). Scale bars represent 50 μm. (**b**–**d**) Example recordings from a 5HT3aR-positive, VIP-positive interneuron (**b**), a 5HT3aR-positive, VIP-negative interneuron (**c**), and a SST interneuron (**d**). Whisking motion was computed from whisker video recordings to define whisking and non-whisking periods (top). Bottom, spikes in the corresponding interneuron type recorded under two-photon guidance in loose-patch configuration. (**e**–**g**) Spiking activity of VIP interneurons and SST interneurons in superficial layers of S1 during active whisking. Whisking onset triggered raster plots of representative VIP (**e**), non-VIP, 5HT3aR (**f**) and SST (**g**) interneurons. Bottom, population PSTHs of VIP, non-VIP, 5HT3aR and SST interneurons. Dotted vertical line at time 0 indicates whisking onset. Dark lines indicate smoothed PSTHs. (**h**) Firing rates of VIP (open circles, 11 cells, 5 mice), non-VIP (gray circles, 5 cells, 3 mice) and SST (black circles, 6 cells, 2 mice) interneurons during whisking plotted against their firing rates during non-whisking periods. Dashed line indicates unity. (**i**)

Firing rates of VIP, non-VIP and SST interneurons during whisking (W) normalized to the firing rates during non-whisking (NW) periods. Each line indicates an individual neuron (VIP interneurons, $P = 0.001$; non-VIP interneurons, $P = 0.94$; SST interneurons, $P = 0.02$). $^{*}P < 0.05$, $^{**}P < 0.005$, Wilcoxon signed-rank test. (**j**) Summary of recording depths of VIP (open circle), non-VIP (gray) and SST (black) interneurons.

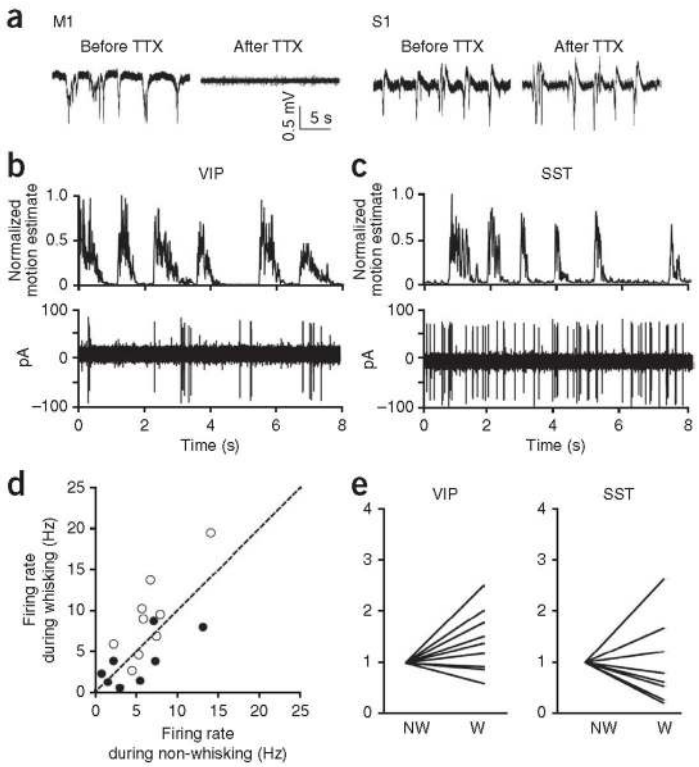

Figure 6.

vM1 activity is responsible for the increased activity of VIP interneurons and decreased activity of SST interneurons in S1 during whisking. (**a**) TTX injection to vM1 silenced the activity of vM1, but did not affect S1 activity, as evidenced by LFPs recorded in S1 and vM1 before and after TTX injection to vM1. TTX injection and LFP recordings were conducted under anesthesia. (**b**,**c**) Representative recordings from a VIP interneuron (**b**) and an SST interneuron (**c**) during vM1 inactivation. Whisking motion was computed from whisker video recordings to define whisking (W) and non-whisking (NW) periods (top). Bottom, spikes in the corresponding interneuron type recorded under two-photon guidance in loose-patch configuration. (**d**) Firing rates of VIP (open circles) and SST (black circles) interneurons during whisking plotted against their firing rates during non-whisking periods after vM1 inactivation. Dashed line indicates unity. (**e**) Summary data comparing firing rates of VIP (9 cells, 2 mice) and SST (8 cells, 3 mice) interneurons during whisking and non-whisking periods after inactivation of vM1 with TTX injection (VIP interneurons, $P = 0.08$; SST interneurons, $P = 0.2$, Wilcoxon signed-rank test).